BIOCHEMISTRY
including biophysical chemistry & molecular biology

Article

pubs.acs.org/biochemistry

Expression, Purification, and Reconstitution of a Diatom Silicon Transporter

Paul Curnow,*[,†] Laura Senior,[†] Michael J. Knight,[†] Kimberlee Thamatrakoln,[‡] Mark Hildebrand,[§] and Paula J. Booth[†]

[†]School of Biochemistry, Medical Sciences Building, University of Bristol, University Walk, Bristol BS8 1TD, U.K.

[‡]Institute of Marine and Coastal Sciences, Rutgers University, New Brunswick, New Jersey 08901, United States

[§]Marine Biology Research Division, Scripps Institution of Oceanography, University of California, San Diego, La Jolla, California 92093, United States

ABSTRACT: The synthesis and manipulation of silicon materials on the nanoscale are core themes in nanotechnology research. Inspiration is increasingly being taken from the natural world because the biological mineralization of silicon results in precisely controlled, complex silica structures with dimensions from the millimeter to the nanometer. One fascinating example of silicon biomineralization occurs in the diatoms, unicellular algae that sheath themselves in an ornate silica-based cell wall. To harvest silicon from the environment, diatoms have developed a unique family of integral membrane proteins that bind to a soluble form of silica, silicic acid, and transport it across the cell membrane to the cell interior. These are the first proteins shown to directly interact with silicon, but the current understanding of these specific silicon transport proteins is limited by the lack of in vitro studies of structure and function. We report here the recombinant expression, purification, and reconstitution of a silicon transporter from the model diatom *Thalassiosira pseudonana*. After using GFP fusions to optimize expression and purification protocols, a His_{10}-tagged construct was expressed in *Saccharomyces cerevisiae*, solubilized in the detergent Fos-choline-12, and purified by affinity chromatography. Size-exclusion chromatography and particle sizing by dynamic light scattering showed that the protein was purified as a homotetramer, although nonspecific oligomerization occurred at high protein concentrations. Circular dichroism measurements confirmed sequence-based predictions that silicon transporters are α-helical membrane proteins. Silicic acid transport could be established in reconstituted proteoliposomes, and silicon uptake was found to be dependent upon an applied sodium gradient. Transport data across different substrate concentrations were best fit to the sigmoidal Hill equation, with a $K_{0.5}$ of 19.4 ± 1.3 μM and a cooperativity coefficient of 1.6. Sodium binding was noncooperative with a K_m^{app} of 1.7 ± 1.0 mM, suggesting a transport silicic acid:Na^+ stoichiometry of 2:1. These results provide the basis for a full understanding of both silicon transport in the diatom and protein−silicon interactions in general.

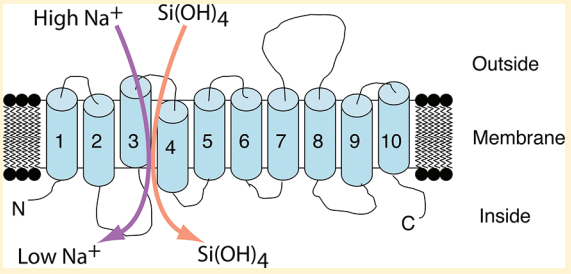

Silicon biomineralization processes are critical to the growth and success of higher plants, sponges, diatoms, silicoflagellates, and other organisms.[1] One particularly interesting example of biosilicification occurs in the diatoms, eukaryotic unicellular algae that surround themselves with an outer cell wall, or frustule, composed largely of amorphous silica. This "glass house" affords the diatoms an ecological advantage, and they constitute ~20% of all of the photosynthetic activity on Earth[2] and fix >200 Tmol of Si/year.[3] They are thus major players in controlling global climate and silicon flux. Different diatom species have radically different frustule morphologies and exert exquisite control over the architecture of these complex biosilica structures at nanometer and micrometer length scales. This remarkable capacity for genetically encoded nanoscale engineering has earned diatoms the sobriquet of "Nature's nanotechnologists"[4] and attracted the attention of scientists and technologists from various disciplines.[5−7]

The process of frustule biosynthesis is gradually becoming better understood, although many aspects are still unclear.[8,9] Diatoms scavenge the soluble form of silica, silicic acid, from low concentrations in the environment. Silicic acid then becomes sequestered into concentrated intracellular pools. The frustule structure is almost completely synthesized inside a specialized silica deposition vesicle in a process that is still being elucidated but involves (poly)peptides,[10] long-chain polyamines,[11] and the cytoskeleton.[12] Upon completion, the frustule is then extruded to the outside of the cell. The mechanism by which silicic acid enters the cell is thus a key component of intracellular frustule biosynthesis. Experimental measurements of silicic acid uptake (for a recent review, see ref 13) and theoretical considerations of silicon requirements[14] strongly suggest that diatoms contain a specialized active transport system for silicic acid, although this has been debated.[15] Surveys of silicon-responsive genes[16−18] have

Received: January 12, 2012
Revised: April 12, 2012
Published: April 24, 2012

   dx.doi.org/10.1021/bi3000484 | *Biochemistry* 2012, 51, 3776−3785

consistently identified a novel family of integral membrane proteins that appear to function as specific silicon transporters (SITs) at the plasma membrane.[18] Uptake assays using microinjected oocytes[16] and diatom membrane vesicles[19] suggest that SIT proteins are silicic acid/sodium symporters with a 1:1 transport stoichiometry. Under low-Si conditions, SIT-mediated uptake of silicic acid in diatom cultures is described by sigmoidal yet saturable kinetics and SITs exhibit a unique high-affinity protein−silicon interaction with values for K_s typically between 0.5 and 10 μM.[20,21] Under high-Si conditions, silicic acid apparently diffuses freely into the cell.[20] The dominant form of silicic acid in seawater is the undissociated monomer $Si(OH)_4$, and current evidence suggests that this is the transported species in marine diatoms.[22]

SITs are ubiquitous among diatoms and generally occur as multiple gene copies that are well-conserved. Analysis of protein sequences suggests that SITs are multipass membrane proteins that comprise ~550 amino acids organized into 10 transmembrane α-helices with a cytoplasmic domain at the carboxyl terminal.[23] Most SITs contain at least part of a canonical sodium binding site and putative conserved GXQ and MXD motifs that are proposed to be involved in silicic acid binding,[23,24] but it is otherwise difficult to infer information about function because the SITs have no sequence similarity to any other proteins. Silicon transporters with unrelated sequences have been identified in rice[25,26] and other higher plants,[27−29] but the functional homology between these and the diatom transporter is unclear; for example, two of the plant transporters identified to date are proposed to function as aquaporin-like channels[25] or silicon/proton antiporters.[26]

A full understanding of silicic acid binding and transport will require a complete description of SIT structure and function at the molecular level. In vitro biochemical and biophysical methods are the most powerful means of acquiring this information. Here, we describe a critical step in this process by establishing protocols for the recombinant expression, purification, and reconstitution of a SIT protein from the model marine diatom *Thalassiosira pseudonana*. We take advantage of these methods to provide the first data for silicic acid transport by a SIT in vitro.

MATERIALS AND METHODS

Molecular Biology. The cDNA sequences of *T. pseudonana* silicon transporters 1−3 were previously cloned into yeast expression plasmid pYES2.[30] This plasmid allows expression from a galactose-inducible promoter, introduces a V5 epitope and His_6 tag at the protein carboxyl terminus, and allows auxotrophic selection. The length of the His tag was increased to His_{10} by PCR-based methods to generate SIT-V5-His_{10} (SIT). The cDNA for GFP from *Astrangia lajollaensis*[31] was kindly provided by P. Daugherty. The GFP cDNA was amplified by PCR using primers with both template and nontemplate sequences to introduce restriction sites for XbaI at the 5′ and 3′ ends of the gene. The forward primer additionally contained a nontemplate linker region comprising a V5 epitope and tobacco etch virus protease (TEV) cleavage site. This PCR product was inserted at the 3′ end of the SIT genes via restriction-based cloning with XbaI to generate SIT-V5-TEV-GFP-His_8 (abbreviated to SIT-GFP). These constructs were transformed by standard methods into protease-deficient *Saccharomyces cerevisiae* strain FGY217 (*ura3-52*, *pep4*Δ)[32] kindly provided by D. Drew, which was used for all expression experiments.

Expression and Purification. Purification was based upon the methods of Li[33] and Newstead.[34] Yeast cultures were grown in −Ura selective medium supplemented with 2% glucose. Protein expression was induced by diluting these cultures to a final OD_{600} of 0.4 in medium supplemented with a 2% galactose/0.1% glucose mixture. After 24 h, cultures were harvested by centrifugation at 3500*g*, and the cell pellet was resuspended in 50 mL of lysis buffer {50 mM Tris-HCl [pH 7.4 at room temperature (RT)], 10% (v/v) glycerol, 150 mM NaCl, and 5 mM EDTA} with 0.1 mg/mL Lyticase, 0.1 mg/mL DNase, and protease inhibitor cocktail (Roche). Cells were lysed by being passed once through a cell disruptor at 30 kpsi. Debris and unlysed cells were removed by centrifugation at 5000*g* for 10 min before the membrane and cytoplasmic fractions were separated by pelleting membranes at 150000*g* for 1 h. Membrane pellets were solubilized in 10−50 mL of membrane solubilization buffer [50 mM Tris-HCl (pH 7.4 RT), 10% (v/v) glycerol, 150 mM NaCl, 100 mM sucrose, protease inhibitors without EDTA, 1% (w/v) Fos-choline-12 (FC-12), and 0.1% (w/v) cholesterol hemisuccinate tris salt (CHS)] for 1 h at 4 °C, and insoluble membranes were removed by repeating the centrifugation at 150000*g*. Imidazole was added to a final concentration of 10 mM, and the soluble supernatant was incubated with Ni^{2+}- or Co^{2+}-charged resins using 1−5 mL column volumes scaled to suit the initial culture volume, for 90 min at 4 °C. The highest yield and purity for the conditions tested were obtained with the TALON cobalt resin (Clontech). Beads were gently pelleted, and the unbound fraction was removed before batch washing with 5 × 10 column volumes of wash buffer [50 mM Tris-HCl (pH 7.4 RT), 10% glycerol, 150 mM NaCl, 10 mM imidazole, protease inhibitors without EDTA, 0.1% (w/v) FC-12, and 0.01% CHS]. Beads were poured into a suitable column, and the final wash was removed under gravity. Purified SIT3 was then eluted in 10 × 0.5 column volumes of elution buffer [50 mM Tris-HCl (pH 7.4 RT), 10% glycerol, 150 mM NaCl, 300 mM imidazole, protease inhibitors without EDTA, 0.1% (w/v) FC-12, and 0.01% CHS]. The sample was immediately concentrated in a centrifugal filter device with a 70 kDa molecular mass cutoff and imidazole removed with a PD-10 desalting column. A detergent-compatible Lowry assay was used to determine the total protein concentration in cell fractions. Size-exclusion chromatography was conducted in 50 mM Tris-HCl (pH 7.4 RT), 10% (v/v) glycerol, 150 mM NaCl, 0.1% (w/v) FC-12, and 0.01% (w/v) CHS using Sephacryl S300HR resin supplied prepacked into a HiPrep 16/60 column (GE Healthcare).

Detergent Screening. All detergents were from Anatrace and of the highest purity. SIT3-GFP membranes were resuspended to a total protein concentration of 2 mg/mL in membrane solubilization buffer without detergent before detergents were added to a final concentration of 1% (w/v). All samples were supplemented with 0.1% CHS. After 1 h, detergent-treated membranes were centrifuged at 150000*g* for 1 h, and the degree of solubilization was determined from the fluorescence of the soluble supernatant relative to the fluorescence of the sample before centrifugation. GFP fluorescence was recorded at an excitation wavelength of 480 nm and emission wavelengths between 495 and 550 nm. The emission maximum was found to be 514 nm.

Electrophoresis. Sodium dodecyl sulfate−polyacrylamide gel electrophoresis (SDS−PAGE) was conducted with precast

dx.doi.org/10.1021/bi3000484 | *Biochemistry* 2012, 51, 3776−3785

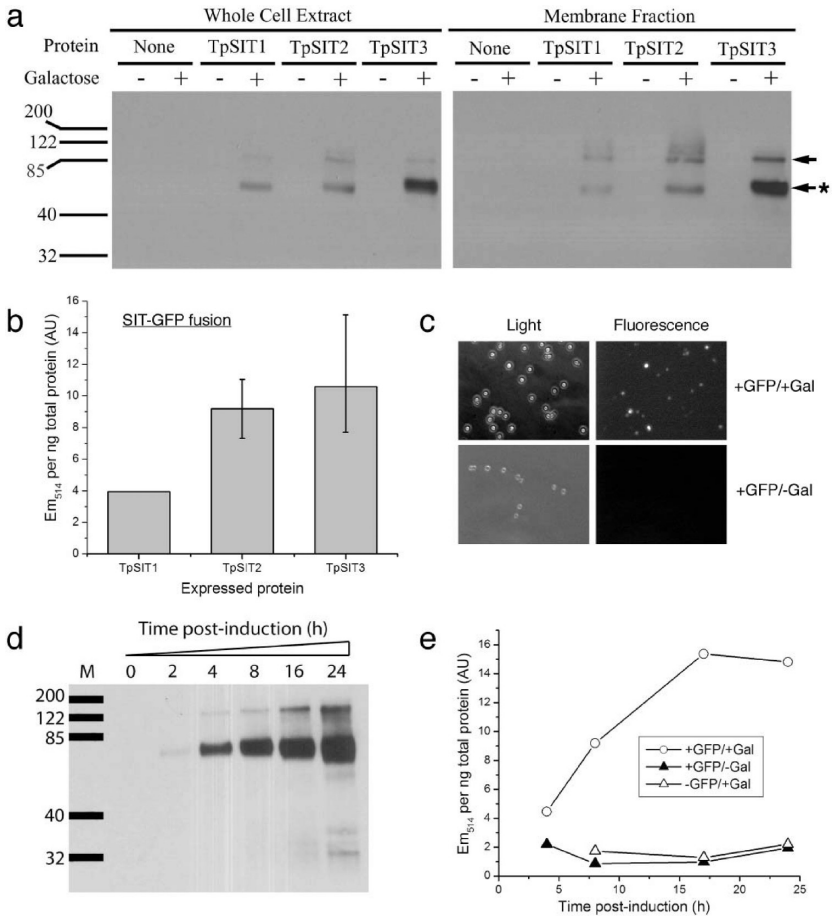

Figure 1. Recombinant expression of SIT and SIT-GFP constructs in the yeast *S. cerevisiae*. Western blotting with anti-V5 (a) showed that all three SITs were expressed and localized to the cell membrane. The position of molecular mass markers is shown at the left (kilodaltons). A major band was observed close to the expected molecular mass of the SITs at 60 kDa (asterisk). The expression of SIT-GFP constructs was determined by quantitative fluorescence spectroscopy (b) and cell imaging (c). Expression was optimal after 16−24 h for both SIT3 (d) and SIT3-GFP (e).

12% acrylamide Tris-HCl gels. Nondenaturing (Native) PAGE used the NativePAGE system (Invitrogen) with precast 4 to 16% Bis-Tris gels. Anti-V5 for Western blotting was from Invitrogen.

Protein Analysis. Particle size analysis was conducted using the Zetasizer Nano from Malvern Instruments. A standard curve was constructed using separate commercial preparations of conalbumin (75 kDa), aldolase (158 kDa), ferritin (440 kDa), and thyroglobulin (669 kDa) at 1 mg/mL in 50 mM Tris-HCl (pH 7.4 and RT), 10% (v/v) glycerol, 150 mM NaCl, 0.1% (w/v) FC-12, and 0.01% (w/v) CHS. Data for SIT3 were collected at 0.5 mg/mL in the same buffer, and size distributions were determined from volume measurements.

Circular dichroism spectra were recorded on a modified Aviv instrument at a protein concentration of 0.14 mg/mL in a 0.05 cm path length cell. The percentage of α-helical content was calculated from the mean residue ellipticity at 222 nm ($[\theta]_{222}$) according to eq 1:[35,36]

$$\%\ \alpha\text{-helix} = 100[(-[\theta]_{222} + 3000)/39000] \quad (1)$$

For transmission electron microscopy, the purified protein was adsorbed to carbon-coated grids and stained with uranyl acetate following the method described by Rubenstein.[37] Microscopy was conducted in the Wolfson Bioimaging Facility at the University of Bristol.

Reconstitution. All experiments were performed using ultrapure water (resistivity of 18.2 MΩ cm at 25 °C) to minimize background silicic acid. Liposomes were formed by dissolving *Escherichia coli* total lipid extract and egg yolk L-α-phosphatidylcholine at a 3:1 weight ratio in chloroform/methanol. The solvent was evaporated by being freeze-dried, and the lipid mixture was resuspended at a lipid concentration of 40 mg/mL in "inside buffer" [50 mM Tris-HCl (pH 7.4 RT), 150 mM KCl, and 100 mM choline chloride] until a smooth suspension was formed. Liposomes were formed by sequential extrusion through 1 and 0.4 μm polycarbonate filters.

SIT3 (2 mg/mL) was mixed with 40 mg/mL liposomes at a 1:20 volumetric ratio (final protein:lipid weight ratio of ~1:500, eight proteins per liposome) and incubated for 20 min at room temperature. Controls without protein were treated with equivalent volumes of 0.1% FC-12 and 0.01% CHS in size-exclusion buffer. Samples were generally used immediately. To assess the degree of reconstitution, proteoliposomes were loaded onto a discontinuous gradient of 50%, 40%, and 0% sucrose at 1:9:1 volumetric ratios and centrifuged at 140000*g* for 1 h. The amount of SIT protein associated with the proteoliposome fraction at the sucrose−buffer interface was determined by immunoblotting.

Silicic Acid Transport Assay. Proteoliposomes were diluted 10-fold into assay buffer [50 mM Tris-HCl (pH 7.4 RT), 150 mM NaCl, and 100 mM choline chloride].

dx.doi.org/10.1021/bi3000484 | *Biochemistry* 2012, 51, 3776−3785

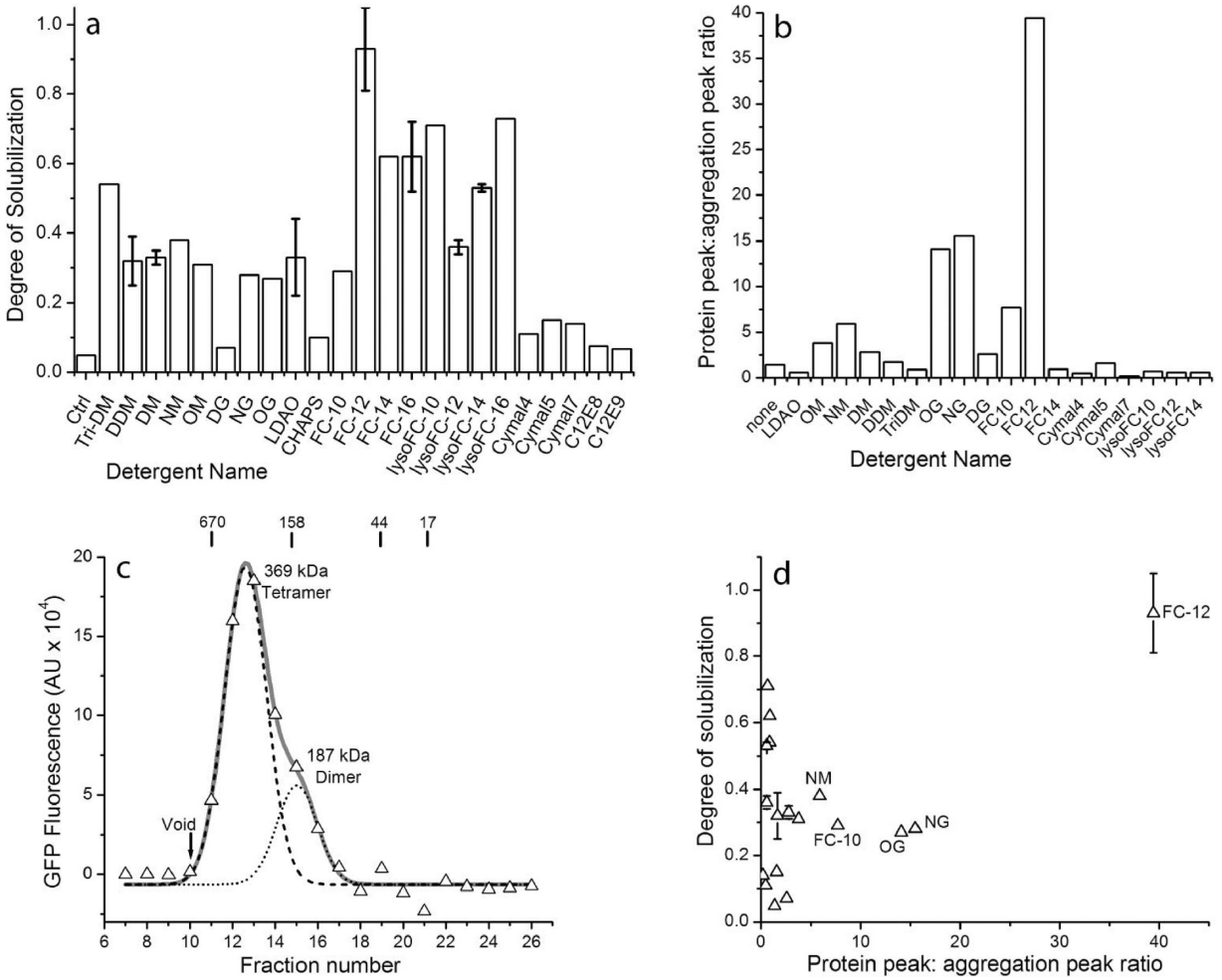

Figure 2. Screening detergent compounds for solubilization and stabilization of SIT3-GFP. (a) FC-12 was found to be most effective at solubilization, consistently extracting >90% of SIT3-GFP from the cell membrane. Error bars, where shown, are differences from the mean average of at least two experiments. (b) Size-exclusion chromatography of most detergent-solubilized membranes gave large aggregate peaks that eluted in the void volume (>1.5 MDa). Comparing the GFP intensity in any eluted peak against fluorescence in the void gives the propensity of the protein to aggregate in that detergent. (c) Size-exclusion chromatogram of FC-12-solubilized membranes expressing SIT3-GFP. The gray line is the combined fit of the two Gaussian functions that give protein molecular masses of 187 kDa (···) and 369 kDa (---), equivalent to SIT3-GFP dimer and tetramer states, respectively. The positions of protein markers are shown above the data with molecular masses in kilodaltons. (d) Plot of data from panel (a) vs data from panel (b) showing the combined performance of the tested detergents in solubility and stability screens.

Monomeric silicic acid was added to this buffer at 0−40 μM by dilution from a concentrated sodium silicate solution. After 5 min at room temperature, proteoliposomes, or empty liposomes in control experiments, were pelleted by centrifugation at 140000*g* for 10 min. The concentration of untransported silicic acid remaining in the supernatant was quantified with the silicomolybdate method of Strickland.[38] Silicomolybdate complexes were formed by incubating samples with acidified ammonium paramolybdate for 10 min before being reduced with 4-(methylamino)phenol hemisulfonate, sulfuric acid, sodium sulfite, and oxalic acid. Color development at 810 nm was measured on a spectrophotometer and calibrated to a standard curve.

Data Analysis. Transport data were fit to a form of the Hill equation:

$$y = y_{max}[S]^n/K_{0.5}{}^n + [S]^n \quad (2)$$

where [S] is the substrate concentration, $K_{0.5}$ is the concentration of substrate at half-y_{max}, and n is the Hill coefficient.

RESULTS

Protein Expression. Three SIT isoforms from *T. pseudonana* were recombinantly expressed in *S. cerevisiae* under the control of a galactose-inducible promoter. SIT1 and SIT2 are highly conserved, being 88% identical and 95% similar in amino acid sequence. SIT3 is less conserved, being 46% identical and 74 and 76% similar to SIT1 and SIT2, respectively.[30] The expression of each of these proteins in yeast was readily detectable in whole-cell and membrane fractions after SDS−PAGE by Western blotting against a C-terminal V5 epitope (Figure 1a). The major band on the immunoblots (labeled with an asterisk) corresponded to a molecular mass of ~60 kDa, close to the expected molecular masses of SIT1 and SIT 2 (both 61 kDa) and SIT3 (65 kDa), with a minor band at 85 kDa. SIT3 appeared to be significantly better expressed than SIT1 or SIT2. Although the reasons for this are unclear, SIT3 does have an extended N-terminal segment that could possibly function as a generic signal sequence, although it is not recognized as such by prediction algorithms such as *SignalP*. Introducing the signal sequence of yeast Invertase at the N-

dx.doi.org/10.1021/bi3000484 | *Biochemistry* 2012, 51, 3776−3785

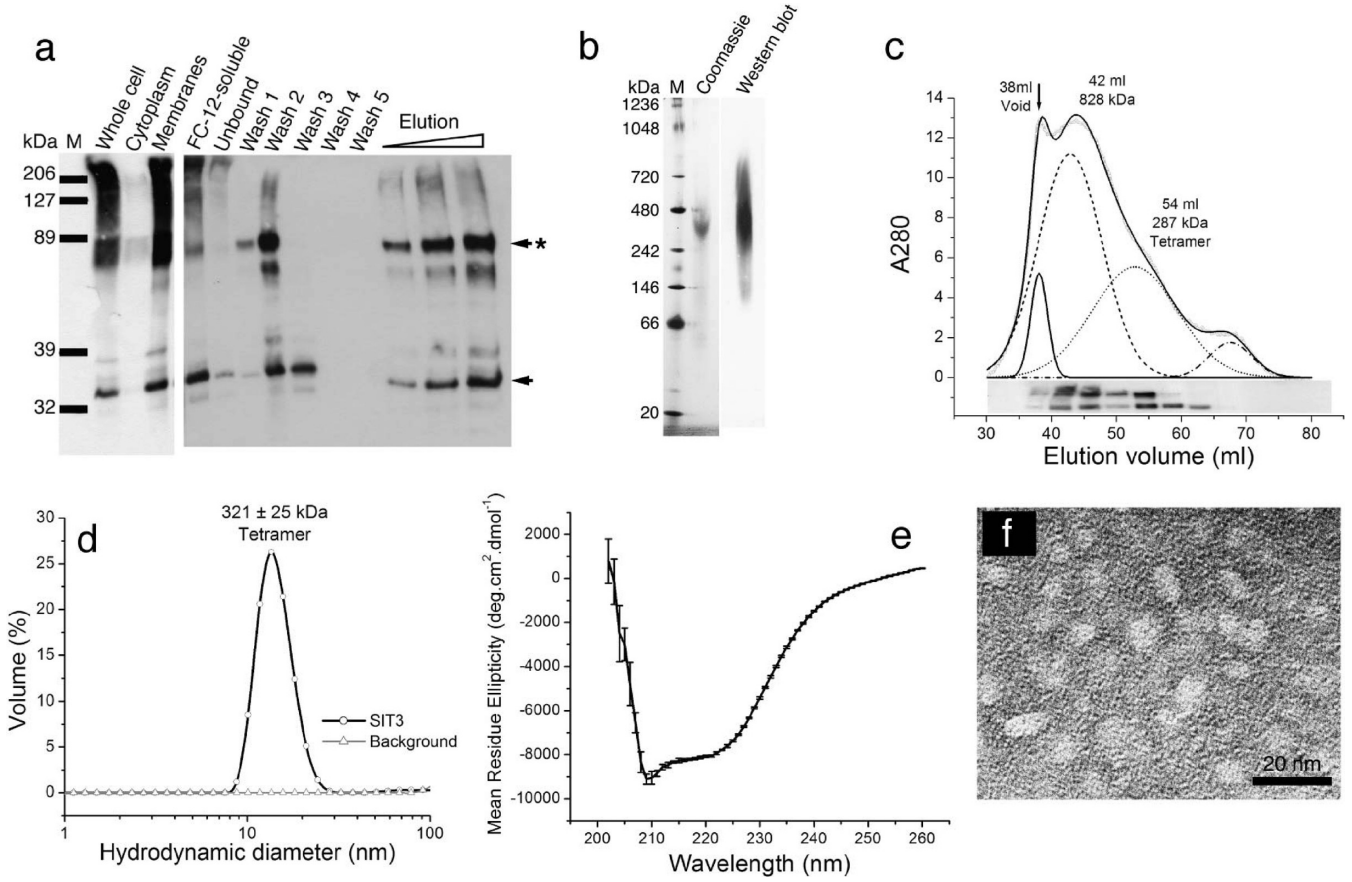

Figure 3. Protein purification and analysis. (a) Western blot of an SDS−PAGE gel with fractions corresponding to each step of SIT3 purification on a Co^{2+} resin: Whole cell, total cell lysate (100 mg of total protein loaded); Cytoplasm, cytoplasmic fraction (100 μg); Membranes, membrane fraction (25 μg); FC-12-soluble, membranes solubilized in the detergent FC-12 (25 μg); Unbound, IMAC column flow-through (25 μg); Washes 1−5, column wash fractions (3, 3, 3, 1.5, and 0.03 μg loaded, respectively); Elution, IMAC column eluent (0.03, 0.06, and 0.09 μg). The first three lanes were collected at shorter exposure time. Lane M contained molecular mass markers (kilodaltons). (b) Native PAGE gel of purified SIT3. Coomassie staining shows a single band at ~290 kDa, equivalent to a protein tetramer. Western blotting confirmed the identity of the band as V5-tagged SIT3. Lane M contained molecular mass markers (kilodaltons). (c) Size-exclusion chromatography shows that the purified protein is prone to aggregation at a relatively high concentration (1.5 mg/mL loaded). Despite this heterogeneity during size exclusion, particle sizing by dynamic light scattering (d) gives a single peak at a molecular mass of 321 ± 25 kDa, consistent with a tetramer. Proteins with known hydrodynamic diameters were used to construct a standard curve for the determination of molecular mass. Secondary structure analysis by circular dichroism (e) shows that purified SIT3 contains the predicted ~35% α-helical structure. Errors are the differences from the mean average of four scans on the same sample. Negative-stain transmission electron microscopy (f) reveals spheroid particles with dimensions of approximately 12 nm × 4 nm.

terminus of SIT2 did not improve expression (data not shown), suggesting that other factors may be responsible for the lower level of expression of this protein. Alternatively, this may reflect differences in the efficiency of protein transfer or the C-terminal epitope could be occluded in SIT1 and SIT2, resulting in a weaker signal upon immunoblotting. No bands were observed in the absence of galactose or in untransformed cell lines, confirming that the antibody was specific to overexpressed SIT proteins. Other antibodies directed toward the C-terminal His tag or an internal protein epitope were unsuccessful, probably because of cross-reactivity with yeast proteins and the inaccessibility of the His tag.

To readily optimize expression, purification, and reconstitution, we introduced a green fluorescent protein (GFP) as a reporter at the carboxyl terminal of the SITs. Introducing GFP at the C-terminus of a membrane protein is generally innocuous and provides a sensitive and quantitative measure of membrane protein expression and purification.[34] Our strategy here was to use SIT-GFP fusions to identify optimal working conditions and then translate these conditions for nonfusion SITs without GFP. GFP from *A. lajollaensis* was introduced at the C-terminus of the SIT proteins via a linker containing a V5 epitope and TEV cleavage site and included a His_8 tag. SIT-GFP fusions were readily expressed in yeast, which was confirmed by fluorimetry on lysed cell samples (Figure 1b) and fluorescence microscopy of live cells (Figure 1c). SIT3-GFP again appeared to give the strongest expression of the three SITs, although the differences in expression between the three SITs were less obvious than on immunoblots.

Following the expression time course of both SIT3 (Figure 1d) and SIT3-GFP (Figure 1e), constructs showed that maximal expression was achieved at approximately 20 h postinduction. Gene expression had no effect on culture growth (not shown). Expression levels were approximately linear with galactose concentration and were not improved via variation of temperature or growth rate (not shown).

Protein Solubilization. The choice of solubilizing detergent is a critically important parameter for studies of membrane proteins in vitro. The fluorescence signal from GFP

dx.doi.org/10.1021/bi3000484 | *Biochemistry* 2012, 51, 3776−3785

fusion proteins can be used to assess the efficiency of different detergents for extracting integral membrane proteins from yeast membranes in a soluble state.[34,39] We conducted a centrifugation-based screen of popular detergent compounds (which vary in aliphatic chain length, chemical and physical properties of the hydrophilic headgroup, aggregation number, critical micelle concentration, and micelle dimensions) that identified Fos-choline-12 (FC-12) as the most effective solubilizing agent for SIT3-GFP, being able to extract >90% of the expressed SIT protein from the yeast cell membrane in a soluble form (Figure 2a). This stringent solubilization screen sediments any unsolubilized membranes and protein aggregates with molecular masses of >800 kDa.

As a measure of the stability of detergent-solubilized protein, detergent-treated membranes were applied to a size-exclusion column (SEC). For many of the samples, the bulk of the GFP fluorescence eluted in the void volume, indicating the formation of nonspecific aggregates larger than 1.5 MDa. Other detergents showed a smaller void peak and a more significant protein peak in later fractions. In each case, the ratio of the fluorescence intensity in the protein peak to the fluorescence in the void peak was calculated.[34] This ratio gives a measure of the propensity toward aggregation in a particular detergent (Figure 2b). FC-12 was again found to be superior to the other compounds tested, giving a minimal void peak and substantial protein peak. This protein peak can be deconvoluted into two components, with a major species at 369 kDa and a minor species at 187 kDa (Figure 2c). These peaks apparently correspond to tetramer and dimer states, respectively, given the expected molecular mass of the SIT3-GFP monomer of 92 kDa and the micelle mass of 25 kDa. Directly comparing solubilization efficiency versus stability (Figure 2d) demonstrates the advantages of FC-12 over the other detergents tested. FC-12 was thus chosen as our detergent of choice for subsequent experiments.

Protein Purification. A decahistidine-tagged SIT3 (without GFP) was purified from FC-12-solubilized membrane extracts by immobilized metal ion affinity chromatography. Figure 3a shows the progress of the purification from the enrichment of SIT3 in fractions of an SDS−PAGE gel, visualized by Western blotting. The column eluent was highly enriched in SIT3. The major band in the purified fraction was again consistent with a monomer at ∼70 kDa. A minor band was also observed in all fractions at ∼35 kDa and presumably arises from limited proteolysis. The overall yield was approximately 0.2 mg of SIT3/L of original yeast culture, and the yield was not improved by adding sucrose or the reducing agent TCEP, changing pH, altering the concentrations of salt or glycerol, or using phosphate buffers (not shown). A Coomassie-stained native PAGE gel (Figure 3b, Coomassie) confirmed the high purity of the protein, showing a single band at approximately 290 kDa. This band was confirmed to be SIT3 by subsequent immunoblotting (Figure 3b, Western blot) and sequencing by mass spectrometry. SIT3 thus purifies in FC-12 as a tetramer, consistent with the results obtained from the detergent screen (Figure 2c).

The IMAC eluate was further purified and analyzed using size-exclusion chromatography. The SEC elution profile was complex and suggested the presence of several oligomeric states (Figure 3c). When the profile was deconvoluted into multiple Gaussian curves, three major protein states were observed: (i) a void peak of protein aggregates >1.5 MDa, (ii) a major peak at a volume corresponding to 828 kDa, corresponding to trimerization of tetramers, and (iii) a smaller peak at 287 kDa, corresponding to SIT3 tetramers. Western blotting of SEC fractions (Figure 3c, bottom profile) confirmed that SIT3 was indeed present in each of these three peaks. The eluted protein continued to run as a monomer on SDS−PAGE gels, although a band corresponding to a dimer at ∼140 kDa was evident in early fractions. This broad distribution of solubilized SIT3 presumably arises from a combination of heterogeneity in the composition and size of protein/detergent micelles and nonspecific oligomerization. This result does not seem to be due to incompatibility with the Sephacryl gel filtration media because similar results were obtained using Sephadex columns. When a similar experiment was performed using SIT3 purified in DDM, only a void peak was observed (not shown), implying more rapid aggregation in this detergent as expected from the experiments depicted in Figure 2.

Particle sizing of purified SIT3 was conducted by dynamic light scattering (Figure 3d). Preparations of SIT3 at 0.5 mg/mL gave a reasonably monodisperse peak with a hydrodynamic diameter of 14.2 nm. A standard curve was constructed from proteins with known hydrodynamic diameters between 75 and 669 kDa in identical buffer and used to determine that the SIT3 had a molecular mass of 321 ± 25 kDa. This further confirms the tetrameric state of SIT3; the aggregation observed in SEC is evidently minimal over the 10 min time course of the light scattering experiment.

Circular dichroism was used to confirm the preservation of α-helical structure in the purified protein. Spectra of SEC-purified protein (Figure 3e) showed that SIT3 was strongly α-helical, with characteristic negative deflections at 208 and 222 nm. It was not possible to collect accurate data below 202 nm because of contributions to the signal by the buffer. Sequence-based computational methods predict that SIT3 will comprise 10 transmembrane α-helices that encompass 210 of the 598 amino acids. The magnitude of the peak at 222 nm is consistent with an exclusively α-helical protein containing ∼35% helical structure (eq 1).

Transmission electron microscopy was used to collect images of the protein−micelle complex. Under negative staining, spheroid particles were observed with dimensions approximately 12 nm × 4 nm (Figure 3f), in reasonable agreement with the expected particle size of 14.2 nm (Figure 3d). The slight discrepancy probably exists because the particle sizing method is optimized for spherical proteins and measures the full hydration shell.

Reconstitution into Proteoliposomes. SIT3 was reconstituted into proteoliposomes at an 8:1 protein monomer:-liposome ratio by a simple dilution method.[40] The success of the reconstitution protocol was determined with a liposome floatation assay that uses a discontinuous sucrose gradient to separate ("float") intact proteoliposomes away from unreconstituted protein. The gradient was split into five fractions, and dot blotting was used to determine the presence of reconstituted protein in each of the fractions (Figure 4, lane PL). The intensity of each dot was calculated with the ImageJ densitometry software,[41] and >85% of the total protein was found to float with the liposome fraction, implying that the reconstitution of proteoliposomes is relatively efficient. Control experiments (Figure 4, lane P) confirmed that in the absence of liposomes the protein remained at the bottom of the gradient.

Functional Assay. SITs are expected to be silicic acid/sodium symporters with a 1:1 transport stoichiometry. The transport activity of reconstituted SIT3 was determined with an

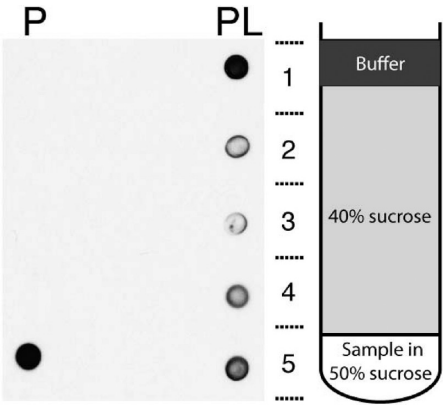

Figure 4. Reconstitution of SIT3 into proteoliposomes. Immunoblotting (dot blot) against the V5 epitope was used to determine the position of protein (lane P) and proteoliposomes (lane PL) on a discontinuous sucrose gradient after centrifugation. The gradient was analyzed in five fractions as shown. In proteoliposome samples, >85% of the protein migrates with liposomes to the buffer boundary.

assay that measures the concentration of silicic acid through its reaction with MoO_4^{2-} to form the blue-colored silicomolybdate, $H_4(SiMo_{12}O_{40})$. Phospholipids interfere with this reaction because of the formation of phosphomolybdates, so it was not possible to analyze proteoliposomes directly for the accumulation of silicic acid. Instead, we measured the depletion of silicic acid from the external medium as it was transported into and sequestered within the proteoliposome lumen.

An inward-directed sodium gradient was established by diluting K^+-containing liposomes or proteoliposomes into Na^+ buffer, and silicic acid was added to the outside of the liposomes at concentrations between 1 and 40 μM. This concentration range was optimal given that silicic acid was previously observed to spontaneously diffuse across lipid bilayers at higher concentrations.[20] Physiological concentrations of silicic acid in ocean surface waters are generally <10 μM,[42] and whole-cell uptake assays have generally used 0−30 μM silicic acid.[20]

Figure 5a shows the results of transport assays at 20 μM silicic acid. A statistically significant (*p = 0.008; n = 6) increase in transport activity over control was only observed for proteoliposomes with an inward-directed sodium gradient (K^+_{in}/Na^+_{out}). This resulted in 1.2 ± 0.9 nmol of silicic acid being transported over control samples. Valinomycin is a potassium channel that allows the rapid egress of K^+ from the liposome interior, causing a charge imbalance and thus generating an electrical membrane potential, $\Delta\Psi$, in addition to the sodium chemical gradient. Preincubating SIT proteoliposomes with valinomycin (K^+_{in}/Na^+_{out}/Val) had no effect on transport activity, confirming that the sodium concentration gradient alone was sufficient to drive silicic acid uptake.[19] Proteoliposomes under K^+_{in}/K^+_{out}, Na^+_{in}/Na^+_{out}, and Na^+_{in}/K^+_{out} conditions were similar to liposomes. These controls confirmed that an inward-directed sodium gradient was required and that the observed uptake was the result of substrate transport rather than substrate binding, the latter of which would be expected to take place in the presence of sodium (Na^+_{in}/Na^+_{out}). The proteoliposome controls also exclude the possibility that uptake is caused simply by an increased leakiness of protein-containing membranes. The presence of K^+ in the assay buffer altered the sensitivity of the assay, but samples could easily be corrected for this solvent

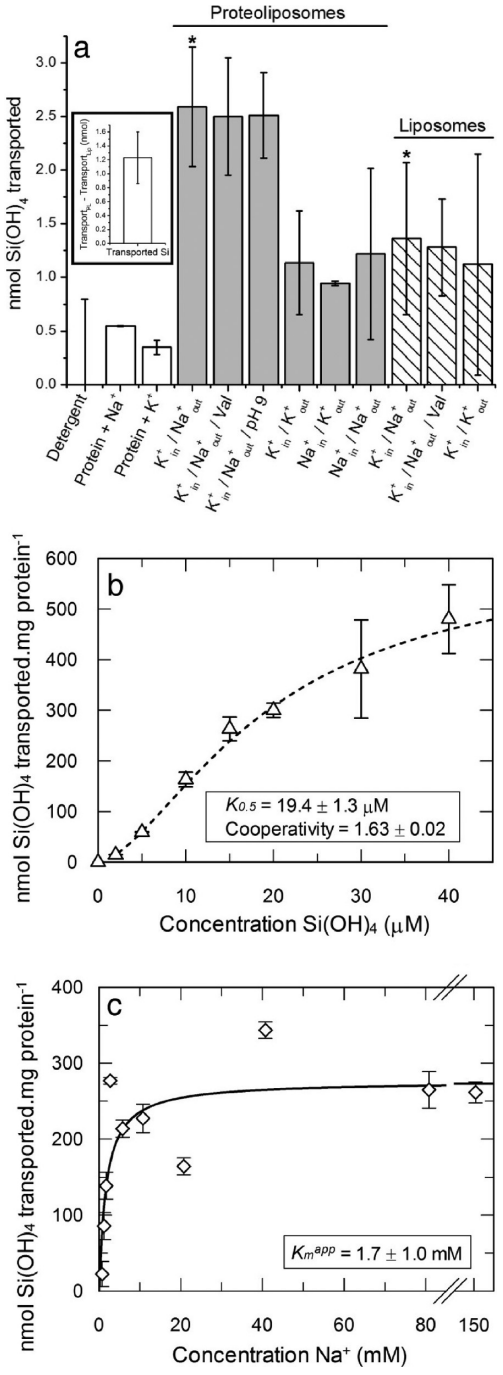

Figure 5. Transport of silicic acid by reconstituted SIT3. (a) Bioenergetics of transport. Proteoliposomes in the presence of an inward-directed sodium gradient (K^+_{in}/Na^+_{out}) transport silicic acid above background levels (*p = 0.008; n = 6). Error bars show the standard deviation from the mean of at least two replicates. All assays were conducted at 20 μM external $Si(OH)_4$. The inset shows the difference in Si uptake between six pairs of proteoliposomes ($Transport_{PL}$) and liposomes ($Transport_{Lip}$) from the same lipid batches. (b) Transport activity is sigmoidal with substrate concentration, suggesting a cooperative process. Each data point is the mean of duplicate experiments with a liposome control background subtracted. The dashed line shows the fit to eq 2. (c) Transport varies with sodium concentration. The solid line shows the best fit to the Michaelis−Menten equation. Data were collected at an external silicic acid concentration of 20 μM.

dx.doi.org/10.1021/bi3000484 | *Biochemistry* 2012, 51, 3776−3785

effect. The assays were performed with three separate protein preparations, with data corrected to account for variations in protein concentration, and across several different liposome preparations. Batch-to-batch variation in liposomes was identified as a major source of variation in the data. Dependent paired *t* tests of samples taken from the same liposome batches gave smaller errors and greater statistical significance (in Figure 5a, $*p = 0.002$; $n = 6$). Comparing relative, rather than absolute, differences between control and treatment groups for each liposome preparation gave 1.2 ± 0.4 nmol of Si transported over background (Figure 5a, inset).

Previous work has shown a pH dependence of silicic acid transport in diatom cultures.[22] Uptake assays of *T. pseudonana* cultures at pH 9.5, where half of the dissolved silicon is ionized to $SiO(OH)_3^-$, gave a V_{max} that was approximately half that of experiments at pH 8.0 where $Si(OH)_4$ predominates. Figure 5a shows that in contrast there are no differences in the in vitro assay of SIT3-driven transport between pH 7.4 (K^+_{in}/Na^+_{out}) and pH 9 (K^+_{in}/Na^+_{out}/pH 9), the high end of the effective pH range of Tris buffer. Given that $pK_1 = 9.47$,[43] the $Si(OH)_4$:$SiO(OH)_3^-$ ratio is 75:25 at pH 9.0. Thus, the bulk ionization state does not appear to influence the total amount of silicic acid transported in vitro.

Measuring uptake across different concentrations of $Si(OH)_4$ gave an apparent sigmoidal trend (Figure 5b). The data are not time-resolved because of difficulties in stopping the reaction, so activity is given here as nanomoles of silicic acid transported per milligram of SIT protein. Fitting this to the Hill equation (eq 2) gave a $K_{0.5}$ of 19.4 ± 1.3 μM, a maximal transport of 601 ± 43 nmol/mg, and a Hill coefficient of 1.6 ± 0.02. The reduced χ^2 value was 0.4. The same data were fit poorly by a Michaelis–Menten hyperbola, with a χ^2 of 414, a maximal transport of 1283 ± 302 nmol/mg, and a $K_{0.5}$ of 67 ± 22 μM. The data are consistent with a recent study of SIT-mediated Si transport in whole cells of *T. pseudonana*, which also showed a sigmoidal trend with Si concentration and gave a $K_{0.5}$ of 8.0 ± 0.9 μM and a Hill slope of 1.9. The in vitro assay developed here and the in vivo assay from an earlier study are thus in relatively close agreement and suggest that SITs bind to silicic acid with moderately high affinity and with some degree of cooperativity.

Figure 5c shows the transport dependence upon sodium concentration. The data were fit to the Michaelis–Menten equation, giving an apparent binding affinity K_m^{app} for Na^+ of 1.7 ± 1.0 mM. This is slightly lower than, but reasonably close to, values obtained for other sodium symporters.[44−47] No cooperativity was evident, indicating a single sodium binding site and suggesting a $Si(OH)_4$:Na^+ transport stoichiometry of 2:1.

DISCUSSION

Silicon is an essential nutrient for many organisms. Diatoms, sponges, radiolaria, and others mineralize siliceous scales, spicules, frustules, and granules as a robust skeletal material for strength and protection. In plants, there is evidence that silicon plays an important structural and biochemical role and it is clear that silicon is crucial in protecting plants from physical, chemical, and biological stress.[44] Silicon has also been implicated as an important trace component of bone and connective tissue in higher animals.[45] Although both plant[46] and diatom[13] silicon transporters have been studied using cell biological methods, the molecular basis of silicon recognition and transport in these systems remains poorly defined. Here, we take the first steps toward a detailed description of the diatom silicon transporter by developing protocols for the expression, purification, and reconstitution of functional SITs in vitro. This establishes the diatom SITs as the first model system for understanding protein–silicon interactions.

Of the three *T. pseudonana* SIT isoforms tested, SIT3 was best expressed in a recombinant yeast cell line (Figure 1a). Interestingly, this is at odds with expression profiling data[17,30] that suggest SIT3 mRNA is present at substantially lower levels compared to the other SITs in the native diatom cell. Additionally expression of SIT3, unlike that of SIT1 and SIT2, does not appear to respond to silicon limitation in the diatom. Nonetheless, the relative similarity of sequence among all three SITs suggests that they share a common structure and function; for example, all three are predicted to have the same structural motif of 10 transmembrane α-helices. This prediction was clearly accurate for SIT3, which was shown here to have a classical α-helical fingerprint in CD measurements (Figure 3e).

A detergent screen was used to identify the optimal conditions for solubilizing and purifying SIT3. Fos-choline and lyso-Fos-choline detergents were more efficient at solubilization from the yeast membrane than the popular maltopyranoside and glucopyranoside compounds. In particular, FC-12 solubilized >90% of SIT3-GFP from the yeast membrane (Figure 2a). FC-12 has previously been noted as being highly efficient for solubilization, but this does not always result in a stable, monodisperse protein.[34] However, size-exclusion chromatography (Figures 2c and 3c), Native PAGE (Figure 3b), and particle sizing (Figure 3d) collectively suggest that SIT3 is purified in FC-12 as a stable tetramer that slowly aggregates at higher concentrations. The only other detergents that performed well in fluorescence size-exclusion chromatography were OG and NG (Figure 2b). It is rather common for integral membrane proteins to be purified as aggregation-prone multimers. Further work is now underway to identify detergents and additives that produce optimal monodisperse preparations that are likely to be more stable and suitable for techniques such as X-ray crystallography. Purifying His_{10}-tagged SIT3 on a cobalt resin yielded 0.2 mg of protein/L of yeast expression culture, similar to the yields reported for other eukaryotic transporters.[34]

Purified protein was reconstituted into synthetic lipsomes by a simple dilution method (Figure 4). This reconstituted protein was active in transporting silicic acid (Figure 5). The most widely used methods for assaying transporter activity measure the accumulation of radiolabeled substrate inside the proteoliposome. The method we describe is the inverse, measuring the depletion of substrate from solution. This approach is feasible in vitro[47] because it is possible to use a relatively high concentration of purified transporters. We found that proteoliposomes with an inward-directed sodium gradient transported 1.2 ± 0.4 nmol of silicic acid over control samples. Because this uptake assay uses ~4.5×10^{11} proteoliposomes, each proteoliposome need only transport ~1600 molecules of silicic acid to achieve the assay results described here.

The reconstituted transporter has an apparent substrate affinity ($K_{0.5}$) of 19.4 ± 1.3 μM. This is similar to, but slightly higher than, values derived from studies of SIT-mediated transport in whole diatom cells (8.0 ± 0.9 μM). Although this disparity could simply arise from differences between the two experimental systems, it raises the intriguing possibility that SIT3 is a low-affinity transporter. Silicon is essential for diatom survival. Transport systems for essential nutrients are generally redundant and feature both low- and high-affinity transporters.

As recently discussed by Levy and colleagues,[48] this provides a competitive advantage because constitutive low-affinity transporters act as an "early warning system" for sensing nutrient starvation; the starvation response includes expression of the high-affinity transporters. This might explain why the sequence of SIT3 diverges from that of SIT1 and SIT2 and why SIT3 is not upregulated under silicon starvation conditions[17] or in response to the cell cycle.[30]

In further agreement with previous experiments, in vitro transport was apparently sigmoidal with substrate concentration, and a fit to these data gave a Hill coefficient of 1.6. This is consistent with the previous conclusion[20] that the transport of $Si(OH)_4$ by *T. pseudonana* SITs is a positively cooperative process, with more than one substrate binding event likely to be required for the completion of the transport cycle. This cooperativity does not appear to be a general property of the silicon transporters because the majority of studies to date report classical hyperbolic uptake kinetics,[19,20] although most of these whole-cell transport assays do not use the low substrate concentrations required to fully describe the early section of a sigmoidal curve. We have not determined the oligomeric state of SIT3 within the bilayer, so cannot say whether the observed cooperativity might be the result of SIT3 oligomerization (Figure 3) or whether the monomer may have multiple substrate binding sites. The orientation of the reconstituted protein within the bilayer is also not known. Potentially, this could be all-inside-out, all-right-side-out, or mixed population of the two. This does not necessarily confound our analysis of the uptake assay because the inward-directed sodium gradient constrains the direction of transport so that efflux should be disfavored. Further work is now underway to determine the orientation and topology of reconstituted SITs.

Bhattacharyya and Volcani studied silicic acid uptake in membrane vesicles from the diatom *Nitzschia alba*[19] and concluded that the $Si(OH)_4$:Na^+ transport stoichiometry was probably 1:1. The in vitro experiments described here imply that, for *T. pseudonana* SIT3, this ratio is 2:1. The suggestion that SIT3 transports two substrate molecules for every sodium ion is congruent with this protein acting as a high-capacity, low-affinity transporter. There are no in vivo data that we know of that we can compare with this result, because the high salt concentrations required to culture marine diatoms have made it difficult to determine the sodium dependence of silicic acid transport in cell culture.

We thus show here that diatom silicon transporters can be recombinantly expressed, purified, and reconstituted in a functional state. This work provides the basis for further investigations into SIT structure and function in vitro.

AUTHOR INFORMATION

Corresponding Author

*E-mail: p.curnow@bristol.ac.uk. Telephone: +44 (0)117 33 12112. Fax: +44 (0)117 33 12168.

Funding

This work was supported by Grant BB/H013032/1 from the UK Biotechnology and Biological Sciences Research Council to P.C. and P.J.B. and European Research Council Starting Grant 282101 under the European Union's Seventh Framework Programme (FP7/2007-2013) to P.C. M.J.K. was supported by the Biochemical Society Guildford Fund, and L.S. is supported by the Bristol Centre for Functional Nanomaterials. P.J.B. is the holder of a Royal Society Wolfson Research Merit Award.

Notes

The authors declare no competing financial interest.

ACKNOWLEDGMENTS

We thank D. Drew for providing yeast strain FGY217, P. Daugherty for the GFP clone, A. Toye for assistance with fluorescence microscopy, and the staff of the University of Bristol Wolfson Bioimaging Facility for assistance with TEM.

ABBREVIATIONS

CHAPS, 3-[(3-cholamidopropyl)dimethylammonio]-1-propanesulfonate; CHS, cholesterol hemisuccinate Tris salt; $C_{12}E_8$, polyoxyethylene (8) dodecyl ether; $C_{12}E_9$, polyoxyethylene (9) dodecyl ether; Cymal 4, 5, and 7, 4-cyclohexyl-1-butyl-, 5-cyclohexyl-1-pentyl-, and 7-cyclohexyl-1-heptyl-β-D-maltopyranoside, respectively; EDTA, ethylenediaminetetraacetic acid; FC-12, Fos-choline-12 (*n*-dodecylphosphocholine); FC-*X*, Fos-choline lipid with aliphatic chain length *X*; GFP, green fluorescence protein from *A. lajollaensis*; IMAC, immobilized metal ion affinity chromatography; LDAO, lauryldimethylamine oxide; Lyso-FC-*X*, lyso-Fos-choline with aliphatic chain length *X*; OG, NG, and DG, *n*-octyl-, *n*-nonyl-, and *n*-decyl-β-D-glucopyranoside, respectively; OM, NM, DM, DDM, and Tri-DM, *n*-octyl-, *n*-nonyl-, *n*-decyl-, *n*-dodecyl, and *n*-tridecyl-β-D-maltopyranoside, respectively; PCR, polymerase chain reaction; SDV, diatom silica deposition vesicle; SEC, size-exclusion chromatography; SIT, diatom silicon transporter; TEV, tobacco etch virus protease; SIT, silicon transport protein from *T. pseudonana* with a V5 eptitope and a His_{10} tag at the C-terminus; SIT-GFP, transcriptional fusion introducing GFP and the His_8 tag at the C-termini of SITs.

REFERENCES

(1) Schröder, H. C., Wang, X., Tremel, W., Ushijima, H., and Müller, W. E. G. (2008) Biofabrication of biosilica-glass by living organisms. *Nat. Prod. Rep. 25*, 455−474.

(2) Field, C. B., Behrenfeld, M. J., Randerson, J. T., and Falkowski, P. (1998) Primary production of the biosphere: Integrating terrestrial and oceanic components. *Science 281*, 237−240.

(3) Treguer, P., Nelson, D. M., van Bennekom, A. J., DeMaster, D. J., Leynaert, A., and Queguiner, B. (1995) The silica balance in the world ocean: A reestimate. *Science 268*, 375−379.

(4) Bradbury, J. (2004) Nature's nanotechnologists: Unveiling the secrets of diatoms. *PLoS Biol. 2*, 1512−1515.

(5) Gordon, R., Losic, D., Tiffany, M. A., Nagy, S. S., and Sterrenburg, F. A. S. (2009) The glass menagerie: Diatoms for novel applications in nanotechnology. *Trends Biotechnol. 27*, 116−127.

(6) Kroger, N. (2007) Prescribing diatom morphology: Toward genetic engineering of biological nanomaterials. *Curr. Opin. Chem. Biol. 11*, 662−669.

(7) Lopez, P. J., Descles, J., Allen, A. E., and Bowler, C. (2005) Prospects in diatom research. *Curr. Opin. Biotechnol. 16*, 180−186.

(8) Kroger, N., and Poulsen, N. (2008) Diatoms: From cell wall biogenesis to nanotechnology. *Annu. Rev. Genet. 42*, 83−107.

(9) Brunner, E., Gröger, C., Lutz, K., Richthammer, P., Spinde, K., and Sumper, M. (2009) Analytical studies of silica biomineralization: Towards an understanding of silica processing by diatoms. *Appl. Microbiol. Biotechnol. 84*, 607−616.

(10) Kroger, N., Deutzmann, R., and Sumper, M. (1999) Polycationic peptides from diatom biosilica that direct silica nanosphere formation. *Science 286*, 1129−1132.

(11) Kroger, N., Deutzmann, R., Bergsdorf, C., and Sumper, M. (2000) Species-specific polyamines from diatoms control silica morphology. *Proc. Natl. Acad. Sci. U.S.A. 97*, 14133−14138.

(12) Tesson, B., and Hildebrand, M. (2010) Extensive and intimate association of the cytoskeleton with forming silica in diatoms: Control over patterning on the meso- and micro-scale. *PloS One 5*, e14300.
(13) Hildebrand, M. (2008) Diatoms, biomineralization processes, and genomics. *Chem. Rev. 108*, 4855−4874.
(14) Thamatrakoln, K., and Kustka, A. B. (2009) When to say when: Can excessive drinking explain silicon uptake in diatoms? *BioEssays 31*, 322−327.
(15) Vrieling, E. G., Sun, Q., Tian, M., Kooyman, P. J., Gieskes, W. W. C., van Santen, R. A., and Sommerdijk, N. A. J. M. (2007) Salinity-dependent diatom biosilicification implies an important role of external ionic strength. *Proc. Natl. Acad. Sci. U.S.A. 104*, 10441−10446.
(16) Hildebrand, M., Volcani, B. E., Gassmann, W., and Schroeder, J. I. (1997) A gene family of silicon transporters. *Nature 385*, 688−689.
(17) Mock, T., Samanta, M. P., Iverson, V., Berthiaume, C., Robison, M., Holtermann, K., Durkin, C., BonDurant, S. S., Richmond, K., Rodesch, M., Kallas, T., Huttlin, E. L., Cerrina, F., Sussman, M. R., and Armbrust, E. V. (2008) Whole-genome expression profiling of the marine diatom *Thalassiosira pseudonana* identifies genes involved in silicon biogenesis. *Proc. Natl. Acad. Sci. U.S.A. 105*, 1579−1584.
(18) Sapriel, G., Quinet, M., Heijde, M., Jourdren, L., Tanty, V., Luo, G., le Crom, S., and Jean Lopez, P. (2009) Genome-wide transcriptome analyses of silicon metabolsim in *Phaeodactylum tricornutum* reveal the multilevel regulation of silicic acid transporters. *PloS One 4*, e7458.
(19) Bhattacharya, P., and Volcani, B. E. (1980) Sodium-dependent silicate transport in the apochlorotic marine diatom *Nitzschia alba*. *Proc. Natl. Acad. Sci. U.S.A. 77*, 6386−6390.
(20) Thamatrakoln, K., and Hildebrand, M. (2008) Silicon uptake in diatoms revisited: A model for saturable and non-saturable uptake kinetics and the role of silicon transporters. *Plant Physiol. 146*, 1397−1407.
(21) Martin-Jezequel, V., Hildebrand, M., and Brzezinski, M. A. (2000) Silicon metabolism in diatoms: Implications for growth. *J. Phycol. 36*, 821−840.
(22) Del Amo, Y., and Brzezinski, M. A. (1999) The chemical form of dissolved Si taken up by marine diatoms. *J. Phycol. 35*, 1162−1170.
(23) Thamatrakoln, K., Alverson, A. J., and Hildebrand, M. (2006) Comparative sequence analysis of diatom silicon transporters: Towards a mechanistic model of silicon transport. *J. Phycol. 42*, 822−834.
(24) Grachev, M. A., Annenkov, V. V., and Likhoshway, Y. V. (2008) Silicon nanotechnologies of pigmented heterokonts. *BioEssays 30*, 328−337.
(25) Ma, J. F., Tamai, K., Yamaji, N., Mitani, N., Konishi, S., Katsuhara, M., Ishiguro, M., Murata, Y., and Yano, M. (2006) A silicon transporter in rice. *Nature 440*, 688−691.
(26) Ma, J. F., Yamaji, N., Mitani, N., Tamai, K., Konishi, S., Fujiwara, T., Katsuhara, M., and Yano, M. (2007) An efflux transporter of silicon in rice. *Nature 448*, 209−212.
(27) Mitani, N., Chiba, Y., Yamaji, N., and Ma, J. F. (2009) Identification and characterization of maize and barley Lsi2-like silicon efflux transporters reveals a distinct silicon uptake system from that in rice. *Plant Cell 21*, 2133−2142.
(28) Chiba, Y., Mitani, N., Yamaji, N., and Ma, J. F. (2009) HvLsi1 is a silicon influx transporter in barley. *Plant J. 57*, 810−818.
(29) Mitani, N., Yamaji, N., and Ma, J. F. (2009) Identification of maize silicon influx transporters. *Plant Cell Physiol. 50*, 5−12.
(30) Thamatrakoln, K., and Hildebrand, M. (2007) Analysis of *Thalassiosira pseudonana* silicon transporters indicates distinct regulatory levels and transport activity through the cell cycle. *Eukaryotic Cell 6*, 271−279.
(31) Bessette, P. H., and Daugherty, P. S. (2004) Flow cytometric screening of cDNA expression libraries for fluorescent proteins. *Biotechnol. Prog. 20*, 963−967.
(32) Kota, J., Gilstring, C. F., and Ljungdahl, P. O. (2007) Membrane chaperone Shr3 assists in folding amino acid permeases preventing precocious ERAD. *J. Cell Biol. 176*, 617−628.
(33) Li, M., Hays, F. A., Roe-Zurz, Z., Vuong, L., Kelly, L., Ho, C. M., Robbins, R. M., Pieper, U., O'Connell, J. D., III, Miercke, L. J. W., Giacomini, K. M., Sali, A., and Stroud, R. M. (2009) Selecting optimum eukaryotic integral membrane proteins for structure determination by rapid expression and solubilization screening. *J. Mol. Biol. 385*, 820−830.
(34) Newstead, S., Kim, H., von Heijne, G., Iwata, S., and Drew, D. (2007) High-throughput fluorescent-based optimization of eukaryotic membrane protein overexpression in *Saccharomyces cerevisiae*. *Proc. Natl. Acad. Sci. U.S.A. 104*, 13936−13941.
(35) MacRaild, C. A., Hatters, D. M., Howlett, G. J., and Gooley, P. R. (2001) NMR structure of human apolipoprotein C-II in the presence of sodium dodecyl sulfate. *Biochemistry 40*, 5414−5421.
(36) Morrow, J. A., Segall, M. L., Lund-Katz, S., Phillips, M. C., Knapp, M., Rupp, B., and Weisgraber, K. H. (2000) Differences in stability among the human apolipoprotein E isoforms determined by the amino-terminal domain. *Biochemistry 39*, 11657−11666.
(37) Rubenstein, J. L. (2007) Structural analysis of membrane protein complexes by single particle electron microscopy. *Methods 41*, 409−416.
(38) Strickland, J. D. H., and Parsons, T. R. (1965) A manual of seawater analysis. *Bull.—Fish. Res. Board Can. 125*, 203.
(39) Kawate, T., and Gouaux, E. (2006) Fluorescence-detection size-exclusion chromatography for precrystallization screening of integral membrane proteins. *Structure 14*, 673−681.
(40) Rigaud, J. L., and Levy, D. (2003) Reconstitution of membrane proteins into liposomes. *Methods Enzymol. 372*, 65−86.
(41) Abramoff, M. D., Magalhaes, P. J., and Ram, S. J. (2004) Image processing with ImageJ. *Biophotonics Int. 11*, 36−42.
(42) Nelson, D. M., Treguer, P., Brzezinski, M. A., Leynaert, A., and Quéguiner, B. (1995) Production and dissolution of biogenic silica in the ocean: Revised global estimates, comparison with regional data and relationship to biogenic sedimentation. *Global Biogeochem. Cycles 9*, 359−372.
(43) Sjöberg, S., Nordin, A., and Ingri, N. (1981) Equilbrium and structural studies of silicon(IV) and aluminium(III) in aqueous solution. II. Formation constants for the monosilicate ions $SiO(OH)_3^-$ and $SiO_2(OH)_2^{2-}$. A precision study at 25 °C in a simplified seawater medium. *Mar. Chem. 10*, 521−532.
(44) Ma, J. F., and Yamaji, N. (2006) Silicon uptake and accumulation in higher plants. *Trends Plant Sci. 11*, 1360−1385.
(45) Jugdaohsingh, R. (2007) Silicon and bone health. *J. Nutr., Health Aging 11*, 99−110.
(46) Ma, J. F., and Yamaji, N. (2008) Functions and transport of silicon in plants. *Cell. Mol. Life Sci. 65*, 3049−3057.
(47) Grinius, L. L., and Goldberg, E. B. (1994) Bacterial multidrug resistance is due to a single membrane protein which functions as a drug pump. *J. Biol. Chem. 269*, 29998−30004.
(48) Levy, S., Kafri, M., Carmi, M., and Barkai, N. (2011) The competetive advantage of a dual-transporter system. *Science 334*, 1408−1412.